

Application of the shift-invert Lanczos algorithm to a non-equilibrium Green function for transport problems

K. Uzawa and K. Hagino

Department of Physics, Kyoto University, Kyoto 606-8502, Japan

Non-equilibrium Green's function theory and related methods are widely used to describe transport phenomena in many-body systems, but they often require a costly inversion of a large matrix. We show here that the shift-invert Lanczos method can dramatically reduce the computational effort. We apply the method to two test problems, namely a simple model Hamiltonian and to a more realistic Hamiltonian for nuclear fission. For a Hamiltonian of dimension 66103 we find that the computation time is reduced by a factor of 33 compared to the direct calculation of the Green's function.

I. INTRODUCTION

To describe transport phenomena in fermionic many-body systems is one of the most important topics in many fields of physics and chemistry [1, 2]. For this purpose, the non-equilibrium Green function (NEGF) and related methods [3–5] have been widely employed as an efficient computational method. For instance, they have been applied to calculate electronic properties of nanodevices, mesoscopic systems, and molecular junctions [6–11]. Recently, the NEGF method has been utilized also to describe nuclear fission reactions as well [12–16].

In this method, one assumes that a system can be divided into two external and an internal systems, and then constructs an effective Hamiltonian for the internal part, in which the couplings to the external parts are taken into account as self-energies. In the cases of electronic devices, the external parts correspond to the semi-infinite electrodes while the internal part is a nano device itself. On the other hand, in the case of nuclear fission reaction, the external parts correspond to decay channels of a nucleus, while the internal part is for mono-nucleus states during a shape evolution of a nucleus. Due to the couplings to the continuum external states, the resultant effective Hamiltonian for the internal part becomes non-Hermitian, and many-body current is allowed to flow between the input and output channels. The transition probability between the channels is calculated using the Green function with the effective Hamiltonian.

While this method is applicable even for cases beyond the linear response theory, the NEGF method requires a significant computational cost, especially for calculations of a Green function, which can be constructed by inverting a Hamiltonian matrix. Notice that the dimension of the Hamiltonian matrix considerably increases with the system size. In the case of silicon nanowire transistors in three-dimension, the matrix dimension becomes orders of 10^5 [17]. As another example, we mention that the dimension is estimated to be orders of 10^6 for neutron induced fission of actinide nuclei [15].

To reduce the numerical costs, specific matrix structures can be useful. For example, under the tight-binding approximation, the Hamiltonian matrix becomes block-tridiagonal, and its inversion can be evaluated by invert-

ing the sub-matrices, instead of the whole matrix [18–21]. This method was applied e.g., in Ref. [17] by dropping off long-range off-diagonal elements due to the electron-phonon coupling. Notice that the applicability of this method is limited by the structure of the considered Hamiltonian. For instance, in the problem discussed in Ref. [17], the Hamiltonian is no longer block-tridiagonal when one takes into account the long-range off-diagonal elements due to the electron-phonon coupling. In the case of nuclear induced fission, a Hamiltonian matrix is in general not block-tridiagonal [15].

To overcome the drawback of the NEGF method, we here discuss the applicability of the Lanczos algorithm [22–24]. The standard Lanczos algorithm provides an efficient method to obtain the ground state of a large matrix. On the other hand, in the NEGF approach, the Green function at various energies has to be evaluated: for which one needs information on the eigenstates in the middle of the spectrum of a Hamiltonian matrix, rather than the ground state. Therefore the usual Lanczos algorithm is not efficient, and we will instead introduce the shift-invert Lanczos algorithm, in which an original eigenvalue equation is transformed to calculate efficiently states in the middle of the spectrum. In this way, the calculation of the NEGF method is accelerated by obtaining specific eigensolutions of a Hamiltonian matrix.

This paper is organized as follows. In Sec. II, we summarize the non-equilibrium Green function method and introduce the shift-invert Lanczos method in the context of the NEGF method. In Sec. III, we numerically demonstrate the efficiency of our approach for a simple schematic model as well as for a more realistic Hamiltonian for fission of ^{236}U based on the density functional theory (DFT). We then summarize the paper in Sec. IV.

II. THE SHIFT-INVERT LANCZOS METHOD FOR NEGF METHOD

A. Non-equilibrium Green's function method

Throughout this paper, we consider a Hamiltonian in a form of,

$$H = \begin{pmatrix} H_L & V_L & 0 \\ V_L^T & H_b & V_R \\ 0 & V_R^T & H_R \end{pmatrix}. \quad (1)$$

This type of Hamiltonian models systems in which the middle part of the Hamiltonian, H_b , is connected to the left and the right parts, H_L and H_R , through V_L and V_R , respectively. In the case of electronic devices, H_L and H_R correspond to Hamiltonians for two electron reservoirs. On the other hand, in nuclear fission, those correspond to Hamiltonians for a compound nucleus configuration and pre-scission configurations, respectively [15, 25]. We assume that there is no direct coupling between H_L and H_R . Generally, the basis vectors are not orthogonal, and we also introduce the overlap matrix for the basis vectors,

$$N_{i,j} = \langle i|j \rangle. \quad (2)$$

The resultant Schrödinger equation becomes a generalized eigenvalue equation,

$$Hf = ENf, \quad (3)$$

where E and f are eigenvalues and eigenvectors, respectively.

When the system is coupled to external channels, one has to add self-energy terms to the Hamiltonian (1) in order to describe decays of the system into the external channels. That is, $H \rightarrow H + \Delta - i\Gamma/2$, where Δ and Γ are the real and imaginary parts of the self-energy originating from the couplings to the external channels. The Hamiltonian matrix then becomes non-Hermitian, and currents are induced. When there are two or more connections to external systems, one can calculate transition probabilities $T_{a,b}$ from a channel a to a channel b using the trace formula [1, 26, 27],

$$T_{a,b}(E) = \text{Tr} [\Gamma_a G(E) \Gamma_b G^\dagger(E)]. \quad (4)$$

Here Γ_a and Γ_b represent decay widths to the corresponding channels, and $G(E)$ is the retarded non-equilibrium Green function defined as,

$$G(E) = \left[EN - \left(H + \Delta - \frac{i}{2}\Gamma \right) \right]^{-1}, \quad (5)$$

where E is the energy of the system.

The quantal trace formula (4) has been widely applied to calculate the electronic properties of nano-devices [1, 11] and cross sections of neutron induced fission [15, 25]. With the Green function $G(E)$, other quantities of a system, such as the spatial density distribution and the level density, can also be evaluated.

Notice that the Green function G is the matrix inverse of the Hamiltonian, and therefore can be diagonalized by the same eigenstates of the Hamiltonian. In the case of non-orthogonal basis, these eigenstates satisfy the equations

$$\left(H + \Delta - \frac{i}{2}\Gamma \right) f_\lambda = \tilde{E}_\lambda N f_\lambda, \quad (6)$$

and

$$\tilde{f}_\lambda^\dagger \left(H + \Delta - \frac{i}{2}\Gamma \right) = \tilde{f}_\lambda^\dagger \tilde{E}_\lambda N. \quad (7)$$

Here λ is the label of eigenstates, f_λ and \tilde{f}_λ are the right-eigenvector and the left-eigenvector, respectively. $\tilde{E}_\lambda \equiv E_\lambda - \frac{i}{2}\Gamma_\lambda$ is a complex eigenvalue for λ . Using these eigenstates, the matrix elements of the Green function are represented in a form of the spectrum decomposition as

$$G_{ij}(E) = \sum_\lambda \frac{(f_\lambda)_i (\tilde{f}_\lambda)_j^*}{E - \tilde{E}_\lambda} = \sum_\lambda \frac{(f_\lambda)_i (\tilde{f}_\lambda)_j^*}{E - E_\lambda + i\Gamma_\lambda/2}. \quad (8)$$

This equation suggests that those eigenstates whose eigenvalue E_λ is close to the energy E dominantly contribute to the Green function due to the energy denominator. This motivates approximating the Green function by a selected set of the eigenstates.

B. Application of the shift-invert Lanczos algorithm

In general, there is a large computational cost to invert a large Hamiltonian matrix. In that circumstance, the spectral decomposition of the Green function may be useful by converting the matrix inversion problem into the eigenvalue problem. As we discussed in the previous subsection, one would need only a few eigenstates to represent the Green function. If the lowest or the highest eigenstates were necessary, one could have used the usual Lanczos algorithm. However, in the problem of NEGF, one needs eigenstates in the middle of the spectrum, and the direct application of the Lanczos algorithm is not efficient. We thus introduce an alternative method with the shift-invert Lanczos algorithm.

In the usual Lanczos algorithm, a symmetric or Hermitian matrix H in an orthogonal basis (that is, $N=1$) is tridiagonalized within the following Krylov subspace [24],

$$\text{span}\{\vec{q}, H\vec{q}, \dots, H^{n-1}\vec{q}\}. \quad (9)$$

Here \vec{q} is an arbitrary initial vector and n is the dimension of the subspace, which can be smaller than the dimension of the matrix H . The tridiagonalized matrix in the

Krylov subspace reads,

$$\begin{pmatrix} \alpha_0 & \beta_1 & & & & \\ \beta_1 & \alpha_1 & \beta_2 & & & \\ & \ddots & \ddots & \ddots & & \\ & & \beta_{n-2} & \alpha_{n-2} & \beta_{n-1} & \\ & & & \beta_{n-1} & \alpha_{n-1} & \end{pmatrix}. \quad (10)$$

It is known that the eigensolutions of the tridiagonal matrix well approximate the eigensolutions of the full Hamiltonian, and the eigensolutions are obtained in the order of the absolute value of eigenvalues¹.

Naively, eigenstates in the middle of the spectrum may be obtained by first transforming the eigenvalue problem $H\psi = E\psi$ to

$$(H - \sigma)^2\psi = (E - \sigma)^2\psi, \quad (11)$$

as suggested in Ref. [28]. Here σ is a real parameter, and thereby the excited states of H with the eigenvalue around σ appear as the lowest eigenstates of $(H - \sigma)^2$. One can then apply the Lanczos algorithm to the matrix $(H - \sigma)^2$ to obtain those eigenstates. However, we found that convergence is sometime slow in this scheme.

We thus advocate using the shift-invert Lanczos algorithm [29]. In this algorithm, the original generalized eigenvalue equation, Eq. (3), is first transformed to

$$(H - \sigma N)f = (E - \sigma)Nf, \quad (12)$$

with a real parameter σ . Then, applying $(E - \sigma)^{-1}(H - \sigma N)^{-1}$ to the both sides of Eq. (12), one obtains

$$(H - \sigma N)^{-1}Nf = (E - \sigma)^{-1}f. \quad (13)$$

Here the original generalized eigenvalue problem is transformed into the eigenvalue problem of the matrix $(H - \sigma N)^{-1}N$, for which eigenvalues around σ have large absolute values due to the form of $(E - \sigma)^{-1}$ on the right hand side of Eq. (13). We solve this eigenvalue problem using the Lanczos iteration. In the iteration, the matrix $(H - \sigma N)^{-1}N$ is applied to the Lanczos vectors, similar to Eq. (9) but with $(H - \sigma N)^{-1}N$ instead of H . The action of N on the Lanczos vectors \vec{v} , $\vec{v}' \equiv N\vec{v}$, is the usual matrix multiplication. In Eq. (13), one needs to evaluate $\vec{x} \equiv (H - \sigma N)^{-1}\vec{v}'$. This is simplified by recognizing that one needs only the action of $(H - \sigma N)^{-1}$ onto the vector \vec{v}' and the inverse of the matrix $(H - \sigma N)$ itself does not need to be obtained. This can be done by firstly factorizing the matrix $(H - \sigma N)$ with e.g. LU factorization and then solving the linear equation,

$$(H - \sigma N)\vec{x} = \vec{v}', \quad (14)$$

for \vec{x} . This method has been implemented in the package ARPACK [30], that is FORTRAN77 numerical software

¹ By adding an appropriate constant matrix to the Hamiltonian, the Lanczos algorithm always yields the ground state solution.

library for solving large-scale eigenvalue problems using the Arnoldi or Lanczos algorithms. In the next section, we demonstrate the effectiveness of this approach using a simple model Hamiltonian as well as a Hamiltonian for fission of ^{236}U nucleus.

III. RESULTS

A. GOE+barrier+GOE model

We first apply our method to a simple model Hamiltonian which has been used in the previous works to discuss the transition state dynamics with a potential barrier [14, 31, 32],

$$H + \Delta = \begin{pmatrix} H_1 & V_1 & 0 \\ V_1^T & B_h & V_2^T \\ 0 & V_2 & H_2 \end{pmatrix}. \quad (15)$$

Here, H_1 and H_2 are random matrices based on the Gaussian Orthogonal Ensemble (GOE) [33–35]. The GOE is characterized by two parameters, the dimension of the matrix N_{GOE} and the size of the matrix elements v . With these parameters, elements of a GOE matrix are given as [33–35],

$$(H_{\text{GOE}})_{i,j} = vr(1 + \delta_{i,j}), \quad (16)$$

where r is a random number sampled from the standard normal distribution. In the calculations shown below, we take $N_{\text{GOE}} = 100$ and $v = 0.1$ in the units of the typical energy scale of the system for both H_1 and H_2 . In this subsection, all quantities related to energy are scaled in a similar way with the typical energy scale of the system.

B_h in Eq. (15) is a real scalar number, corresponding to the height of a barrier. The GOE matrices and the barrier configuration are connected with vectors V_1 and V_2 . The elements of V_1 and V_2 are random numbers sampled from the normal distribution with the mean value of zero and the standard deviation of 0.1². In this model, the basis vectors are orthogonal, and the overlap matrix N becomes the unit matrix.

We assume that H_1 is connected to two different kinds of external channels, the input channel Γ_{in} and the left output channels Γ_{L} . On the other hand, H_2 is assumed to connect to the right output channels Γ_{R} .³ We assume that the decay matrices corresponding to these channels are given by,

$$(\Gamma_{\text{in}})_{k,k'} = \gamma_{\text{in}}\delta_{k,1}\delta_{k',1}, \quad (17)$$

² We have confirmed that our conclusion remains the same even when all the matrix elements of V_1 and V_2 are fixed to a constant number, 0.1, although the convergence with respect to the number of eigenstates to be included becomes somewhat slower.

³ In the problem of neutron induced fission reactions, Γ_{in} , Γ_{L} , and Γ_{R} correspond to a neutron channel, capture channels, and fission channels, respectively.

$$\Gamma_L = \begin{pmatrix} \gamma_L I & 0 & 0 \\ 0 & 0 & 0 \\ 0 & 0 & 0 \end{pmatrix}, \quad (18)$$

and

$$\Gamma_R = \begin{pmatrix} 0 & 0 & 0 \\ 0 & 0 & 0 \\ 0 & 0 & \gamma_R I \end{pmatrix}, \quad (19)$$

where I is the unit matrix with the dimension of N_{GOE} . With this set up, the trace formula (4) for the transition probabilities is transformed to

$$T_{\text{in,R}} = \gamma_{\text{in}} \gamma_R \sum_{j \in \text{R}} |G_{1,j}|^2. \quad (20)$$

and

$$T_{\text{in,L}} = \gamma_{\text{in}} \gamma_L \sum_{j \in \text{L}} |G_{1,j}|^2. \quad (21)$$

Using the spectrum decomposition of the Green function, the transition probability $T_{a,b}$ in these equations reads,

$$T_{a,b} = \gamma_a \gamma_b \sum_{\lambda} \frac{|(f_{\lambda})_a|^2 |(\tilde{f}_{\lambda})_b|^2}{(E - E_{\lambda})^2 + (\Gamma_{\lambda}/2)^2} + \gamma_a \gamma_b \sum_{\lambda \neq \lambda'} \frac{(f_{\lambda})_a (f_{\lambda'})_a^* (\tilde{f}_{\lambda})_b (\tilde{f}_{\lambda'})_b^*}{(E - \tilde{E}_{\lambda})(E - \tilde{E}_{\lambda'})^*}. \quad (22)$$

In the actual numerical calculations, we take $\gamma_{\text{in}} = 1.25 \times 10^{-3}$, $\gamma_L = 3.25 \times 10^{-3}$, and $\gamma_R = 1 \times 10^{-3}$, which are much smaller than the real parts of the Hamiltonian matrix elements, $v = 0.1$ in Eq. (16). We take $B_h=2$ and set the excitation energy $E = 0$. Since the values of γ are small, one can perturbatively treat the decay matrix $\Gamma = \Gamma_{\text{in}} + \Gamma_R + \Gamma_L$ to evaluate the eigenstates of the non-Hermitian matrix $H + \Delta - i\Gamma/2$. That is, we first solve the Schrödinger equation without the imaginary part as

$$(H + \Delta)f_{\lambda} = E_{\lambda} N f_{\lambda}, \quad (23)$$

and then evaluate the imaginary part of the eigenvalues approximately as

$$\Gamma_{\lambda} = \sum_i |(f_{\lambda})_i|^2 \Gamma_{ii}. \quad (24)$$

Notice that with this treatment the right-eigenvector f and the left-eigenvector \tilde{f} in Eqs. (6) and (7) do not need to be evaluated separately, because those coincide with each other for a Hermitian matrix, $H + \Delta$.

The dimension of the Hamiltonian matrix in our calculation is 201, which is small enough to easily evaluate the Green function by the direct matrix inversion. Let us then compare the transmission coefficients obtained by the direct method to those with the shift-invert Lanczos method. For the latter calculations, we obtain k eigenstates around the energy E by setting $\sigma = E$, and use

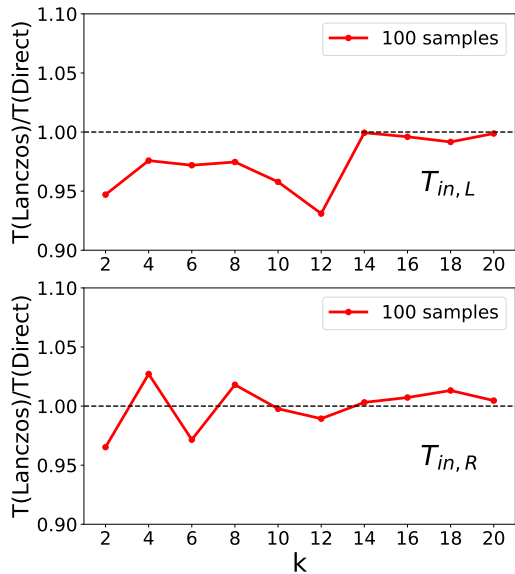


FIG. 1. The ratio of transmission coefficients for the Hamiltonian in Eq.(15) at $E = 0$ with parameters defined in the text, calculated by the two methods. The number of eigenstates k included in shift-invert Lanczos method is shown on the horizontal axis. The results for $T_{\text{in,L}}$ and $T_{\text{in,R}}$ are shown in the upper and lower panels, respectively.

these k eigenstates to calculate the transmission coefficients $T_{\text{in,L}}$ and $T_{\text{in,R}}$ by reducing the summation in Eq. (22) as

$$\sum_{\lambda} \rightarrow \sum_{\lambda=1}^k. \quad (25)$$

Since the model uses the GOE ensemble, we need to average over sample matrices to evaluate physical quantities. With our setup, we find that 100 samples provides sufficient convergence properties⁴. The ratios of the transition probabilities at $E = 0$ calculated with the shift-invert Lanczos method to those with the direct method are shown in Fig.1 as a function of the number of eigenstates k obtained by the shift-invert Lanczos method. To this end, we follow Ref. [30] and randomly generate the elements of the initial vector \vec{q} for the Lanczos algorithm. For each of the 100 samples, we use a different initial vector. The upper and the lower panels of Fig. 1 show the results for $T_{\text{in,L}}$ and $T_{\text{in,R}}$, respectively. In the cases with 1 sample (not shown), the transition coefficients obtained with the shift-invert Lanczos method do not converge even with large values of k . As the sample number increases, the ratios become close to one. With 100 samples, the error becomes less than 1% for both $T_{\text{in,L}}$ and $T_{\text{in,R}}$ at $k = 20$.

⁴ We have confirmed that the results are not significantly altered by using other sets of 100 samples

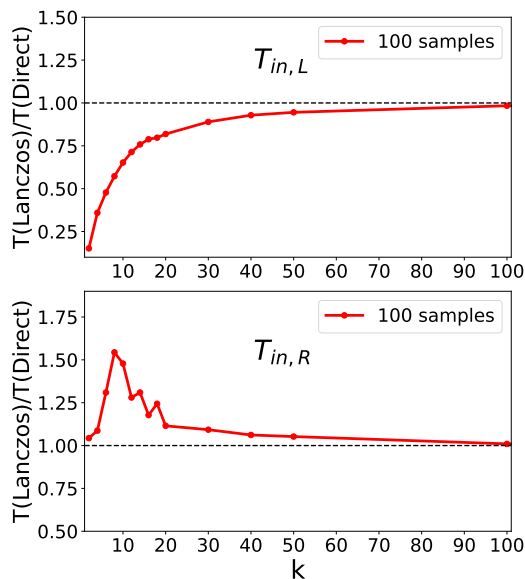


FIG. 2. Same as Fig.1, but for larger values of the width parameters (see the main text). The horizontal axis k is the number of eigenstates obtained by the shift-invert Arnoldi method.

We next consider a case where γ_{in} , γ_{L} , and γ_{R} are not small so that resonances are overlapping with each other. In this case, the approximation in Eqs. (23) and (24) is not justified, and one needs to solve the eigenvalue equation for the Hamiltonian $H + \Delta - \frac{i}{2}\Gamma$ as it is. The Lanczos algorithm is no longer applicable to such non-Hermitian Hamiltonian, and the Arnoldi algorithm, which is a generalization of the Lanczos algorithm, has to be applied [30]. Figure 2 shows the results for $\gamma_{\text{in}} = \gamma_{\text{L}} = \gamma_{\text{R}} = 0.1$, while the other parameters are set to be the same as before. One can see that the transmission coefficients with the Arnoldi algorithm are converged to those with the direct calculations when the value of k is large enough, even though a larger value of k is required as compared to the case with isolated resonances shown in Fig. 1. The slower convergence can be easily understood with Eq. (22), which indicates that the more eigenstates contribute for the larger values of widths.

B. ^{236}U with seniority zero configurations

We next apply the same procedure to a more realistic case, that is, neutron induced fission of ^{236}U nucleus. To this end, we calculate the Hamiltonian matrix of ^{236}U based on the nuclear DFT [36–38]. The employed Hamiltonian is the same as that used in the previous work [25], in which the details of the model Hamiltonian can be found.

In the DFT calculation, we consider many-particle many-hole configurations at a given nuclear shape along a fission path. To generate such configurations, we first

solve the Kohn-Sham equations by constraining the expectation value of the mass-quadrupole moment

$$Q = \int d\mathbf{r} \rho(\mathbf{r}) Y_{20}(\hat{\mathbf{r}}), \quad (26)$$

where $\rho(\mathbf{r})$ is the mass-distribution of nucleons and Y_{20} is the spherical-Harmonics function. In our calculations, the fission path is discretized such that the overlap between the neighboring configurations is e^{-1} [15, 25]. As a consequence, we have 14 reference points from the ground state deformation to a deformation prior to scission. The value of Q for those reference points are summarized in Table I. Notice that there are first and second barriers along the fission path, as shown in Fig. 1 in Ref. [25].

At each reference point, we generate particle-hole excited configurations up to $E_{\text{max}} = 5$ MeV, for each of proton and neutron excitations. The dimension of a Hamiltonian at each Q (i.e., “ Q -block”) is also summarized in Table I. As in the previous subsection, we replace the left-most and the right-most blocks by GOE matrices $H_{\text{GOE}}^{(L)}$ and $H_{\text{GOE}}^{(R)}$. For the GOE parameters, we take $N_{\text{GOE}} = 1000$ and $v = 0.32$ MeV. The off-diagonal elements of the Hamiltonian matrix are evaluated according to a monopole pairing interaction and the diabatic interaction [25]. We neglect the couplings among Q -blocks beyond the nearest neighboring, and therefore the Hamiltonian matrix becomes block-tridiagonal as,

$$H = \begin{pmatrix} H_{\text{GOE}}^{(L)} & V_L & & & \\ V_L^T & H_1 & V_{1,2} & & O \\ & V_{2,1} & H_2 & V_{2,3} & \\ & & & \ddots & \\ O & & V_{11,12} & H_{12} & V_R \\ & & & V_R^T & H_{\text{GOE}}^{(R)} \end{pmatrix}. \quad (27)$$

Here H_i represents the Hamiltonian matrix at each quadrupole moment, Q_i , and $V_{i,i+1}$ represents the off-diagonal Hamiltonian matrix between the Q blocks i and $i+1$.

Similarly to the previous subsection, based on the shift-invert Lanczos method for the trace formula, Eq. (4), we calculate the transition probabilities $T_{n,\text{cap}}$ and $T_{n,\text{fis}}$ at $E = 6.5$ MeV, which is equal to the neutron separation energy in ^{236}U [39]. We use the same partial widths to those in Sec. III A, for which Γ_{in} , Γ_{L} and Γ_{R} correspond to Γ_n , Γ_{cap} and Γ_{fis} , respectively. Following Ref. [25], we set $\gamma_n = 0.01$ MeV, $\gamma_{\text{cap}} = 0.00125$ MeV, and $\gamma_{\text{fis}} = 0.015$ MeV. Similarly to the previous subsection, Γ_n has one diagonal component in the left-most block, while Γ_{cap} and Γ_{fis} have N_{GOE} diagonal components in the left-most and the right-most blocks, respectively. In the shift-invert Lanczos calculation, we set $\sigma = 6.5$ MeV.

Fig. 3 shows the ratios of the transition probabilities calculated with the shift-invert Lanczos method to those with the direct method. The calculations were performed using a single node equipped in Yukawa-21 supercomputer at the Yukawa Institute for Theoretical Physics

TABLE I. The quadrupole moment Q and the dimension of each Q -block along a fission path of ^{236}U . The quadrupole moment is given in units of barn. The total dimension is 66103 with $N_{\text{GOE}} = 1000$.

Q (barn)	14	18	23	29	34	39	46	51	57	62	67	74	79	83
dimension	N_{GOE}	2520	9794	15088	11577	2774	2940	3021	3150	2196	3752	2871	4420	N_{GOE}

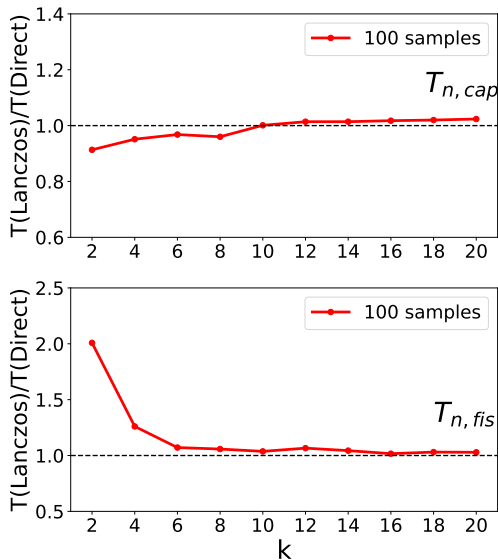


FIG. 3. Similar to Fig.1, but for the transition probabilities at $E=6.5$ MeV for fission of ^{236}U . For the shift-invert Lanczos method, we set $\sigma = 6.5$ MeV.

(YITP), Kyoto University. We apply the ZGETRF and ZGETRI subroutines included in Lapack [40] for the calculations of the matrix inversion. On the other hand, the ARPACK library is used for the calculation of shift-invert Lanczos Algorithm [30]. By taking an ensemble average with 100 samples, the error of our approach is smaller than 3% for both capture and fission, as shown by the red lines in the figure. Moreover, one can also observe that the results are almost converged with $k = 10$. That is, we need only as small as 10 eigenstates to represent the Green function, whose dimension is 66103.

Let us next discuss computation times needed to compute the Green function for fission of ^{236}U ,

$$G(E) = \left(EN - \left(H - \frac{i}{2}\Gamma \right) \right)^{-1}. \quad (28)$$

In the following calculations, we fix the left-end and the right-end GOE matrices and increase the number of the intermediate subblocks H_i and $V_{i,i+1}$ one by one. The real calculation times and CPU times needed for the calculations are shown in the upper and the lower panels in Fig. 4 as a function of the matrix dimension, respectively. As shown in the upper panel, the shift-invert Lanczos method reduces the real computational time in all the cases. For the dimension of 66103, the shift-invert Lanczos method is faster by a factor of about 33.4 as compared

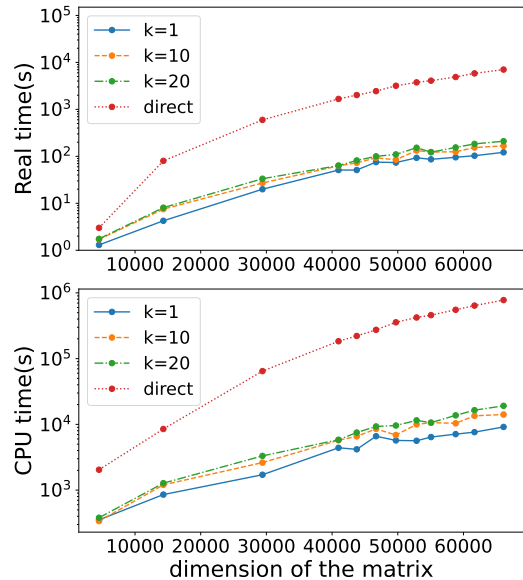


FIG. 4. (The upper panel) The real computational time for the shift-invert Lanczos method and the direct matrix inversion. To draw this figure, the left-end and the right-end GOE matrices are fixed and the number of intermediate Q -blocks is increased one by one. The quantity k in the legend denotes the number of eigenvectors calculated with the shift-invert Lanczos method. See the text for details of the numerical calculations. (The lower panel) Similar to the upper panel, but for the CPU times.

to the direct matrix inversion. The result is similar for the CPU time shown in the lower panel, although the ratio of the CPU times is increased to about 40.3. The computation times are summarized in Table II. Notice that the computational cost of the direct matrix inversion increases as $O(N^3)$, while that for the shift-invert Lanczos method changes much weakly. Therefore, the shift-invert Lanczos method provides a powerful tool for transport phenomena, especially when the dimension of a Hamiltonian is large.

IV. SUMMARY

We have discussed the applicability of the shift-invert Lanczos approach for the NEGF method. In the shift-invert Lanczos approach, the Green function is expressed in a form of the spectrum decomposition with eigenvalues and eigenstates of a generalized eigenvalue equation. As only those eigenstates around E contribute to transition probabilities, the shift-invert Lanczos approach can be

TABLE II. The computational times required to compute the Green function with the direct matrix inversion method and with the shift-invert Lanczos method.

	dimension	direct	shift-invert Lanczos		
			$k=1$	$k=10$	$k=20$
Real time(s)	4520	3.59	1.18	1.51	1.89
	43753	2.01×10^3	5.11×10	7.26×10	8.17×10
	66103 (full)	7.03×10^3	1.22×10^2	1.67×10^2	2.10×10^2
CPU time(s)	4520	2.04×10^3	3.35×10^2	3.42×10^2	3.81×10^2
	43753	2.21×10^5	4.17×10^3	6.57×10^3	7.51×10^3
	66103 (full)	7.77×10^5	9.14×10^3	1.41×10^4	1.93×10^4

applied to obtain such eigenstates efficiently. We have demonstrated that such approach reproduces the exact result by the direct inversion of a matrix with good accuracy for both a simple schematic model and for a more realistic case of fission of ^{236}U nucleus. We have also demonstrated that the computation time can be considerably reduced, e.g., by a factor of about 30 for the fission problem of ^{236}U .

For the problem of fission, so far we have restricted the model space only to seniority zero configurations, that is, all nucleons are assumed to form time-reversal pairs. In more realistic calculations, it is essential to include also finite seniority configurations. A serious problem towards such calculations is that the dimension of a Hamiltonian matrix can be as huge as $O(10^6)$ [15]. In such occasion,

the shift-invert Lanczos approach discussed in this paper shall provide a promising tool.

ACKNOWLEDGMENTS

We thank G.F. Bertch for useful discussions and for a careful reading of the manuscript. This work was supported in part by JSPS KAKENHI Grant No. JP23K03414 and JP23KJ1212. The numerical calculations were performed through the use of SQUID at the Cybermedia Center, Osaka University and Yukawa-21 at Yukawa Institute for Theoretical Physics, Kyoto University.

-
- [1] S. Datta, *Electronic Transport in Mesoscopic Systems* (Cambridge University Press, Cambridge, 1995).
- [2] S. Datta, *Quantum Transport: Atom to Transistor* (Cambridge University Press, 2005).
- [3] P. Danielewicz, Quantum theory of nonequilibrium processes, i, *Annals of Physics* **152**, 239 (1984).
- [4] K. Balzer and M. Bonitz, *Nonequilibrium Green's Functions Approach to Inhomogeneous Systems* (Springer, 2012).
- [5] G. Stefanucci and R. van Leeuwen, *Nonequilibrium Many-Body Theory of Quantum Systems: A Modern Introduction* (Cambridge University Press, 2013).
- [6] M. B. Nardelli, Electronic transport in extended systems: Application to carbon nanotubes, *Phys. Rev. B* **60**, 7828 (1999).
- [7] J. Taylor, H. Guo, and J. Wang, Ab initio modeling of quantum transport properties of molecular electronic devices, *Phys. Rev. B* **63**, 245407 (2001).
- [8] P. S. Damle, A. W. Ghosh, and S. Datta, Unified description of molecular conduction: From molecules to metallic wires, *Phys. Rev. B* **64**, 201403 (2001).
- [9] M. Brandbyge, J.-L. Mozos, P. Ordejón, J. Taylor, and K. Stokbro, Density-functional method for nonequilibrium electron transport, *Phys. Rev. B* **65**, 165401 (2002).
- [10] Y. Xue, S. Datta, and M. A. Ratner, First-principles based matrix green's function approach to molecular electronic devices: general formalism, *Chemical Physics* **281**, 151 (2002).
- [11] M. Thoss and F. Evers, Perspective: Theory of quantum transport in molecular junctions, *The Journal of Chemical Physics* **148**, 030901 (2018).
- [12] Y. Alhassid, G. Bertsch, and P. Fanto, Addendum to "Derivation of K-matrix reaction theory in a discrete basis formalism", *Ann. Physics* **424**, 168381 (2021).
- [13] G. F. Bertsch and K. Hagino, Generator coordinate method for transition-state dynamics in nuclear fission, *Phys. Rev. C* **105**, 034618 (2022).
- [14] H. A. Weidenmüller, Random-matrix approach to transition-state theory, *Phys. Rev. E* **105**, 044143 (2022).
- [15] G. F. Bertsch and K. Hagino, Modeling fission dynamics at the barrier in a discrete-basis formalism, *Phys. Rev. C* **107**, 044615 (2023).
- [16] K. Uzawa and K. Hagino, Schematic model for induced fission in a configuration-interaction approach, *Phys. Rev. C* **108**, 024319 (2023).
- [17] M. Luisier and G. Klimeck, Atomistic full-band simulations of silicon nanowire transistors: Effects of electron-phonon scattering, *Phys. Rev. B* **80**, 155430 (2009).
- [18] K. S. Dy, S.-Y. Wu, and T. Spratlin, Exact solution for the resolvent matrix of a generalized tridiagonal hamiltonian, *Phys. Rev. B* **20**, 4237 (1979).
- [19] E. M. Godfrin, A method to compute the inverse of an n-block tridiagonal quasi-hermitian matrix, *Journal of Physics: Condensed Matter* **3**, 7843 (1991).
- [20] A. Svizhenko, M. P. Anantram, T. R. Govindan, B. Biegel, and R. Venugopal, Two-dimensional quantum mechanical modeling of nanotransistors, *Journal of Applied Physics* **91**, 2343 (2002).
- [21] D. Petersen, H. Sørensen, P. Hansen, S. Skelboe, and K. Stokbro, Block tridiagonal matrix inversion and

- fast transmission calculations, *Journal of Computational Physics* **227**, 3174 (2008).
- [22] C. Lanczos, An iteration method for the solution of the eigenvalue problem of linear differential and integral operators, *Journal of Research of the National Bureau of Standards* **45**, 10.6028/jres.045.026 (1950).
- [23] C. Lanczos, Solution of systems of linear equations by minimized iterations¹, *Journal of research of the National Bureau of Standards* **49**, 33 (1952).
- [24] J. K. Cullum and R. A. Willoughby, *Lanczos Algorithms for Large Symmetric Eigenvalue Computations* (Society for Industrial and Applied Mathematics, 2002).
- [25] K. Uzawa and K. Hagino, Nonequilibrium green's function approach to low-energy fission dynamics: Fluctuations in fission reactions, *Phys. Rev. C* **110**, 014321 (2024).
- [26] Y. Meir and N. S. Wingreen, Landauer formula for the current through an interacting electron region, *Phys. Rev. Lett.* **68**, 2512 (1992).
- [27] W. H. Miller, Beyond transition-state theory: a rigorous quantum theory of chemical reaction rates, *Accounts of Chemical Research* **26**, 174 (1993), <https://doi.org/10.1021/ar00028a007>.
- [28] G. Grosso, L. Martinelli, and G. Pastori Parravicini, Lanczos-type algorithm for excited states of very-large-scale quantum systems, *Phys. Rev. B* **51**, 13033 (1995).
- [29] T. Ericsson and A. Ruhe, The spectral transformation lanczos method for the numerical solution of large sparse generalized symmetric eigenvalue problems, *Mathematics of Computation* **35**, 1251 (1980).
- [30] R. B. Lehoucq, D. C. Sorensen, and C. Yang, *ARPACK Users' Guide* (Society for Industrial and Applied Mathematics, 1998) <https://epubs.siam.org/doi/pdf/10.1137/1.9780898719628>.
- [31] K. Hagino and G. Bertsch, Microscopic derivation of transition-state theory for complex quantum systems, *Journal of the Physical Society of Japan* **93**, 064003 (2024).
- [32] H. Weidenmüller, Transition-state theory reexamined, *Phys. Rev. E* **109**, 034117 (2024).
- [33] T. A. Brody, J. Flores, J. B. French, P. A. Mello, A. Pandey, and S. S. M. Wong, Random-matrix physics: spectrum and strength fluctuations, *Rev. Mod. Phys.* **53**, 385 (1981).
- [34] H. A. Weidenmüller and G. E. Mitchell, Random matrices and chaos in nuclear physics: Nuclear structure, *Rev. Mod. Phys.* **81**, 539 (2009).
- [35] G. E. Mitchell, A. Richter, and H. A. Weidenmüller, Random matrices and chaos in nuclear physics: Nuclear reactions, *Rev. Mod. Phys.* **82**, 2845 (2010).
- [36] N. Schunck, ed., *Energy Density Functional Methods for Atomic Nuclei*, 2053-2563 (IOP Publishing, 2019).
- [37] T. Nakatsukasa, K. Matsuyanagi, M. Matsuo, and K. Yabana, Time-dependent density-functional description of nuclear dynamics, *Rev. Mod. Phys.* **88**, 045004 (2016).
- [38] M. Bender, P.-H. Heenen, and P.-G. Reinhard, Self-consistent mean-field models for nuclear structure, *Rev. Mod. Phys.* **75**, 121 (2003).
- [39] L. C. Leal, H. Derrien, N. M. Larson, and R. Q. Wright, R-Matrix Analysis of ²³⁵U Neutron Transmission and Cross-Section Measurements in the 0- to 2.25-keV Energy Range, *Nucl. Sci. Eng.* **131**, 230 (1999).
- [40] E. Anderson, Z. Bai, C. Bischof, S. Blackford, J. Demmel, J. Dongarra, J. Du Croz, A. Greenbaum, S. Hammarling, A. McKenney, and D. Sorensen, *LAPACK Users' Guide*, 3rd ed. (Society for Industrial and Applied Mathematics, Philadelphia, PA, 1999).